Cancer Research

Temozolomide Induces Senescence and Repression of DNA Repair Pathways in Glioblastoma Cells via Activation of ATR–CHK1, p21, and NF-κB

Dorthe Aasland, Laura Götzinger, Laura Hauck, Nancy Berte, Jessica Meyer, Melanie Effenberger, Simon Schneider, Emelie E. Reuber, Wynand P. Roos, Maja T. Tomicic, Bernd Kaina, and Markus Christmann

Abstract

The DNA-methylating drug temozolomide, which induces cell death through apoptosis, is used for the treatment of malignant glioma. Here, we investigate the mechanisms underlying the ability of temozolomide to induce senescence in glioblastoma cells. Temozolomide-induced senescence was triggered by the specific DNA lesion O^6-methylguanine (O^6MeG) and characterized by arrest of cells in the G_2–M phase. Inhibitor experiments revealed that temozolomide-induced senescence was initiated by damage recognition through the MRN complex, activation of the ATR/CHK1 axis of the DNA damage response pathway, and mediated by degradation of CDC25c. Temozolomide-induced senescence required functional p53 and was dependent on sustained p21 induction. p53-deficient cells, not expressing p21, failed to induce senescence, but were still able to induce a G_2–M arrest. p14 and p16, targets of p53, were silenced in our cell system and did not seem to play a role in temozolomide-induced senescence. In addition to p21, the NF-κB pathway was required for senescence, which was accompanied by induction of the senescence-associated secretory phenotype. Upon temozolomide exposure, we found a strong repression of the mismatch repair proteins MSH2, MSH6, and EXO1 as well as the homologous recombination protein RAD51, which was downregulated by disruption of the E2F1/DP1 complex. Repression of these repair factors was not observed in G_2–M arrested p53-deficient cells and, therefore, it seems to represent a specific trait of temozolomide-induced senescence.

Significance: These findings reveal a mechanism by which the anticancer drug temozolomide induces senescence and downregulation of DNA repair pathways in glioma cells.

Introduction

The success of cancer therapy with genotoxic anticancer drugs rests on their potency to induce cell death. However, genotoxic anticancer drugs not only induce death, but are also effective in activating other pathways such as cellular senescence, which allows cancer cells to survive without proliferation (1). In a previous study, we have shown that glioblastoma cells treated with the methylating anticancer drug temozolomide undergo apoptosis and, in the same dose range and time period, senescence (2). Evidence for induction of senescence by temozolomide was also provided in other studies with glioma cells (3–5). The finding that not all tumor cells can be killed through anticancer drug treatment is of importance in view of the dismal prognosis of patients with glioblastoma with a median survival of 14.6 months and the 2-year survival rate less than 26.5% (6).

Temozolomide is being used as first-line monotherapeutic in glioblastoma therapy, applied after resection and usually concomitant with radiotherapy (6). Temozolomide exerts its cytotoxic effect by the induction of O^6-methylguanine (O^6MeG), which ultimately leads to the formation of DNA double-strand breaks (DSB) and cell death (7). The success of glioma therapy is strongly determined by the DNA repair capacity of a tumor. Thus, the cytotoxic DNA lesion O^6MeG is subject to repair by the DNA repair enzyme O^6-methylguanine-DNA methyltransferase (MGMT). In the absence of MGMT, O^6MeG persists in the DNA and mispairs with thymine during DNA replication, resulting in GC→AT transition mutations. In addition to its mutagenic potential, O^6MeG can be converted via DNA replication and futile DNA mismatch repair (MMR) into DSBs in the second replication cycle after temozolomide exposure. If these DSBs are not repaired, they result in chromosomal aberrations and the activation of cell death pathways (7). DSBs can be repaired by homologous recombination (HR) and/or nonhomologous end joining (NHEJ). The repair of radiation-induced DSBs occurs mainly via NHEJ, whereas temozolomide-induced DSBs are repaired by HR (8). Cells that are deficient in MGMT or impaired in HR are highly sensitive to temozolomide (8), whereas cells that express MGMT and lack MMR are resistant (7).

Department of Toxicology, University Medical Center Mainz, Mainz, Germany.

Note: Supplementary data for this article are available at Cancer Research Online (http://cancerres.aacrjournals.org/).

Corresponding Authors: Markus Christmann, University Medical Center Mainz, Obere Zahlbacher Str. 67, Mainz D-55131, Germany. Phone: 49-6131-179066; Fax: 49-6131-178499; E-mail: mchristm@uni-mainz.de; Bernd Kaina, kaina@uni-mainz.de; and Maja T. Tomicic, tomicic@uni-mainz.de

doi: 10.1158/0008-5472.CAN-18-1733

As shown by extensive *in vitro* studies, temozolomide-induced death of glioma cells results mainly from apoptosis (9–11). However, temozolomide was also shown to induce at the same time autophagy and senescence (2). Senescence induced by temozolomide was suggested to be dependent on p53 and CHK1/CDC25c–dependent G_2–M arrest (3, 4). Temozolomide also induces apoptosis and senescence in glioma cells cultured as multicellular spheroids (5). The role of DNA damage–induced senescence in glioblastoma therapy is less clear. It is pertinent to speculate that senescent cancer cells escape therapy and contribute to recurrent tumor growth, which usually occurs following glioma radiochemotherapy. Senescence was initially described as a permanent cell-cycle arrest involved in limiting the lifespan of cultured human fibroblasts (12). Contrary to quiescence, which is defined as a temporary cell-cycle arrest, senescence cannot be reversed by proliferative stimuli. This general statement is, however, doubted by recent publications, showing that under specific conditions, cells could escape senescence (13–15). Cellular senescence is induced by telomere shortening (replicative senescence), proliferation-associated signals (oncogenic senescence), or by genomic damage caused, among others, by anticancer drugs (DNA damage–triggered senescence). In the latter case, senescence is dependent on sustained DNA damage response (DDR) signaling, provoked very likely by unrepairable DNA lesions (16).

As senescence may have a serious impact on therapy, we attempted to study in more detail the mechanism of temozolomide-induced senescence in glioma cells. In extension of our previous work (2), we analyzed the impact of the specific temozolomide-induced DNA lesion O^6MeG and the DDR triggered by this critical lesion on the induction of cell-cycle arrest and senescence. Furthermore, we addressed the question whether in temozolomide-induced senescent glioma cells the DNA repair capacity is altered compared with nonsenescent cells. The data show that the temozolomide-induced DNA damage O^6MeG is the main trigger of senescence, which is initiated by activation of the MRN–ATR–CHK1 pathway and is dependent on CDC25c degradation. In addition to this, activation of p21 and NF-κB is required, but not of p14 or p16. Temozolomide-induced senescence was accompanied by disruption of the E2F1/DP1 complex, which leads to downregulation of the DNA repair factors EXO1, MSH2, MSH6, and RAD51. The high potency of the temozolomide-induced damage O^6MeG to trigger senescence may explain the lack of curability of gliomas treated with this anticancer drug.

Materials and Methods

Cell culture, drug treatment, and siRNA-mediated knockdown

The glioma cell lines [LN229 (RRID:CVCL_0393), LN229-MGMT, U87 (RRID:CVCL_0022), LN308 (RRID:CVCL_0394), and U138 (RRID:CVCL_0020)] were cultivated in DMEM containing 10% FBS in a humidified atmosphere containing 7% CO_2 at 37°C. U87 cells were purchased from Cell Line Service and the glioblastoma cell line LN229 was obtained from LGC Standards. Both cell lines are deficient for MGMT expression due to promoter methylation and also show no MGMT activity as determined by the radioactive MGMT assay (17). LN229-MGMT cells were stably transfected with MGMT cDNA showing strong MGMT expression and activity (2). All cell lines were regularly checked for MGMT activity. LN308 and U138 cells were kindly provided by Prof. Weller (Laboratory of Molecular Neuro-Oncology, University Hospital and University of Zurich, Zurich, Switzerland) and were characterized (18). MGMT-transfected LN229 cells were described previously (2).

All cells were kept in culture for no longer than 2 months and were regularly checked for *Mycoplasma* contamination using the VenorGEM Classic Detection Kit (catalog no. 11-1,100) from Minerva Biologicals. All lines were characterized in the laboratory of origin, displayed the expected phenotype, but were not reauthenticated in our laboratory.

Temozolomide was purchased from Prof. Geoff Margison, Centre for Occupational and Environmental Health, University of Manchester, Manchester, United Kingdom. The NF-κB inhibitors III (CAS 380623-76-7; Merck Millipore) and JSH23 (CAS 749886-87-1; Selleckchem) were used at 10 μmol/L and 50 μmol/L, respectively. The CHK1 inhibitor UCN-01 (CAS 112953-11-4; Sigma Aldrich) was used at 50 nmol/L, the CHK1 inhibitor MK8776 (CAS 891494-63-6; Selleckchem) was used at 0.5–2 μmol/L, the CHK2 inhibitor II hydrate (CAS 516480-79-8; Sigma Aldrich) was used at 10 μmol/L, and the p21 inhibitor UC2288 (CAS 532813; Calbiochem) was used at 5 μmol/L. The ATM inhibitor KU60019 (CAS 925701-49-1; Selleckchem) was used at 10 μmol/L, the ATR inhibitor VE-821 (CAS 1232410-49-9; Selleckchem) was used at 10 μmol/L, the DNA-PKcs inhibitor KU0060648 (CAS, 881375-00-4; Selleckchem) was used at 900 μmol/L, and the MRN inhibitor Mirin (CAS 1198097-97-0; Tocris) was used at 25 μmol/L. For silencing of p21, predesigned siRNA (sc-29427; Santa Cruz Biotechnology) and control human nonsilencing siRNA (Silencer Select Predesigned siRNA Negative Control #1 siRNA; Ambion) were used. Silencing of CHK1 was performed using predesigned siGENOME SMARTpool siRNA (M-003255-04; Dharmacon). The transfections of siRNAs were performed using Lipofectamine RNAiMAX Reagent (Invitrogen).

Xenograft experiments

To induce subcutaneous xenografts, U87 cells (2.5×10^6) were injected in the left and the right flank of 4 female immunodeficient mice (BALB/cAnNRj-*Foxn1*$^{nu/nu}$, Janvier Labs). When tumors reached a suitable size (22 mm^3), two randomly selected animals were injected with temozolomide (200 mg/kg body weight in DMSO/NaCl, i.p.) and two with solvent, respectively. Ninety-six hours later the mice were sacrificed and tumors were isolated, immediately frozen in liquid nitrogen, and stored at −80°C. For expression analysis, the left and right tumors were combined and the tissue was disintegrated using a tissue lyser (Retsch). Whole-cell protein extract was isolated as described previously (19) and concentration was measured according to the Bradford method. Animal experiments were performed in accordance with relevant institutional and national guidelines and regulations, and were approved by the Landesuntersuchungsamt Rheinland Pfalz, Germany (23 177-07/041-15V2).

Preparation of RNA and qRT-PCR

Total RNA was isolated using the Nucleo Spin RNA Kit (Machery and Nagel). One microgram total RNA was transcribed into cDNA (Verso cDNA Kit, Thermo Fisher Scientific) and qPCR was performed using the GoTaq qPCR Master Mix Protocol (Promega) and the CFX96 Real-Time PCR Detection System (Bio-Rad). In all experiments, qPCR was performed in technical triplicates, SD shows intraexperimental variation. The analysis was performed using CFX Manager Software. Nontranscribed controls were

included in each run, expression was normalized to *gapdh* and *β-actin*; the untreated control was set to one. The specific primers are listed in Supplementary Table S1.

Immunoprecipitation and chromatin immunoprecipitation

Immunoprecipitation was performed using the Catch and Release v2.0 Kit (Merck) according to the manufacturer's protocol. ChIP was performed as described previously (20). qRT-PCR was performed using specific primers flanking the E2F1-binding site of *EXO1*, *MSH2*, *MSH6*, and *RAD51*, which are listed in Supplementary Table S1.

Determination of apoptosis and cell-cycle progression

For monitoring drug-induced apoptosis, Annexin V-FITC/propidium iodide (PI)–double stained cells were analyzed by flow cytometry. To determine cell-cycle distribution, cells were incubated for different times after temozolomide exposure. Harvested samples were prepared as follows: Following 30-minute RNA digestion with 0.1 mg/mL RNase in PBS, they were stained with PI and cell-cycle distribution was determined by flow cytometry using a BD FACSCanto II. Experiments were repeated at least three times, mean values ± SD are shown.

Determination of senescence and isolation of senescent cells

For detection of senescence, cells were washed twice with PBS, afterwards fixed with 2% formaldehyde, 0.2% glutaraldehyde in PBS. After washing with PBS, cells were stained (40 mmol/L citric acid/phosphate buffer pH 6.0, 150 mmol/L NaCl, 2 mmol/L $MgCl_2$, 5 mmol/L potassium ferrocyanide, 5 mmol/L potassium ferricyanide, 0.1% x-Gal) overnight at 37°C. Cells were then washed with PBS and overlaid with 70% glycerine. Micrographs were acquired and analyzed using the Cell A Imaging Software (Olympus) in combination with a Zeiss Axiovert 35 microscope. A total of 500–1,000 cells were analyzed per sample. In all cases, experiments were repeated at least three times; mean values ± SD are shown. For flow cytometry–based detection of senescence, cells were exposed to temozolomide for indicated times. Thereafter, medium was removed and 4-mL fresh medium containing 10% FCS and 300 μmol/L chloroquine was added per 10-cm dish. Cells were incubated for 30 minutes at 37°C. Finally, 33 μmol/L C_{12}FDG (ImaGene Green C12FDG lacZ Gene Expression Kit) was added and incubated for 90 minutes at 37°C. The medium was removed, cells were washed with PBS, trypsinized, and resuspended in PBS. Senescence was measured at the BD FACSCanto II flow cytometer. For isolation of senescent cells, the cells were resuspended in dissociation buffer (Gibco) containing 1% FCS and C_{12}FDG-positive cells were sorted using a BD FACS Aria sorter.

Preparation of protein extracts and Western blot analysis

Whole-cell and nuclear extracts were prepared as described previously (19). For Western blot analysis using phospho-specific antibodies, cells were directly lysed in 1× SDS-PAGE sample buffer and subsequently sonified. Mouse mAbs were diluted 1:500–1:1,000 in 5% BSA, 0.1% Tween-TBS, and incubated overnight at 4°C. Rabbit pAbs were diluted 1:2,000 and incubated for 2 hours at room temperature. The protein–antibody complexes were visualized by Pierce ECL Western Blotting Substrate (Thermo Fisher Scientific). The specific antibodies are listed in Supplementary Table S2.

MMR and HR activity assay

For MMR-specific electromobility shift assay, 29-nucleotide oligomers with the sequence 5′-GGGCTCGAGCTGCAGCTGCTAGTAGATCT-3′ were annealed to oligomers with the sequence 5′-GGGAGATCTACTAGNAGCTGCAGCTCGAG-3′ (n = C or T) and labeled with [^{32}P]dATP using polynucleotide kinase. Nuclear extracts were prepared and incubated with the oligomers as described previously (21). DNA-protein complexes were separated in 4% polyacrylamide gels. The efficiency of HR was determined by a qPCR-based HR Assay Kit (Norgen Biotek Corporation), as described previously (11). Cells were exposed to 100 μmol/L temozolomide; 72 hours later the cells were transfected with the HR plasmids and 24 hours thereafter subjected to isolation of total cellular DNA. Samples were standardized with universal primers, detecting the plasmid backbone for control of transfection efficiency.

Quantification and statistical analysis

The data were evaluated using Student *t* test and were expressed as mean ± SD. *, $P \leq 0.05$ was considered statistically significant, **, $P \leq 0.01$ very significant, ***, $P \leq 0.001$ highly significant, and ****, $P \leq 0.0001$ most significant. Statistical analyses were performed using GraphPad Prism version 6.01 for Windows, GraphPad Software (www.graphpad.com).

Results

Senescence following temozolomide is dependent on O^6MeG and triggered by the MRN–ATR pathway

Previously, we showed that O^6MeG is the initial trigger of temozolomide-induced apoptosis, which is mediated through the DDR (22). To analyze whether this is also true for the activation of senescence, the DDR factors ATM, ATR, MRN, and DNA-PKcs were pharmacologically inhibited and the frequency of senescence was measured in LN229 cells (proficient for p53 and deficient for MGMT) by scoring senescence-associated β-galactosidase (β-Gal)–positive cells (Fig. 1A). To identify the senescence-inducing DNA lesions, activation of senescence was also measured in LN229 cells that express MGMT following transfection with MGMT cDNA (LN229-MGMT). The data show that senescence was induced only in MGMT-deficient LN229 glioma cells, but not in the MGMT-proficient LN229-MGMT isogenic cell line (Fig. 1A). Because the isogenic lines only differ in the MGMT repair capacity and, thereby, the amount of O^6MeG following temozolomide treatment, we conclude that this lesion is not only responsible for inducing temozolomide-induced cell death (9), but also for senescence. The inhibitor experiments revealed that temozolomide-induced senescence in MGMT-deficient cells is dependent on ATR, but not ATM. In addition to ATR, inhibition of MRN and DNA-PKcs also protected against temozolomide-induced senescence, indicating that the MRN complex and DNA-PKcs are involved.

Temozolomide-induced senescence is activated in the G_2–M cell-cycle phase

To mimic the clinical situation, repeated exposure to temozolomide (25 and 50 μmol/L) at 5 consecutive days was performed. In addition, a combined treatment schedule using temozolomide (25 μmol/L) and IR (2 Gy) was applied. The data revealed that repeated low-dose temozolomide exposure is highly efficient in inducing senescence in p53-proficient U87 (up to 60%) and

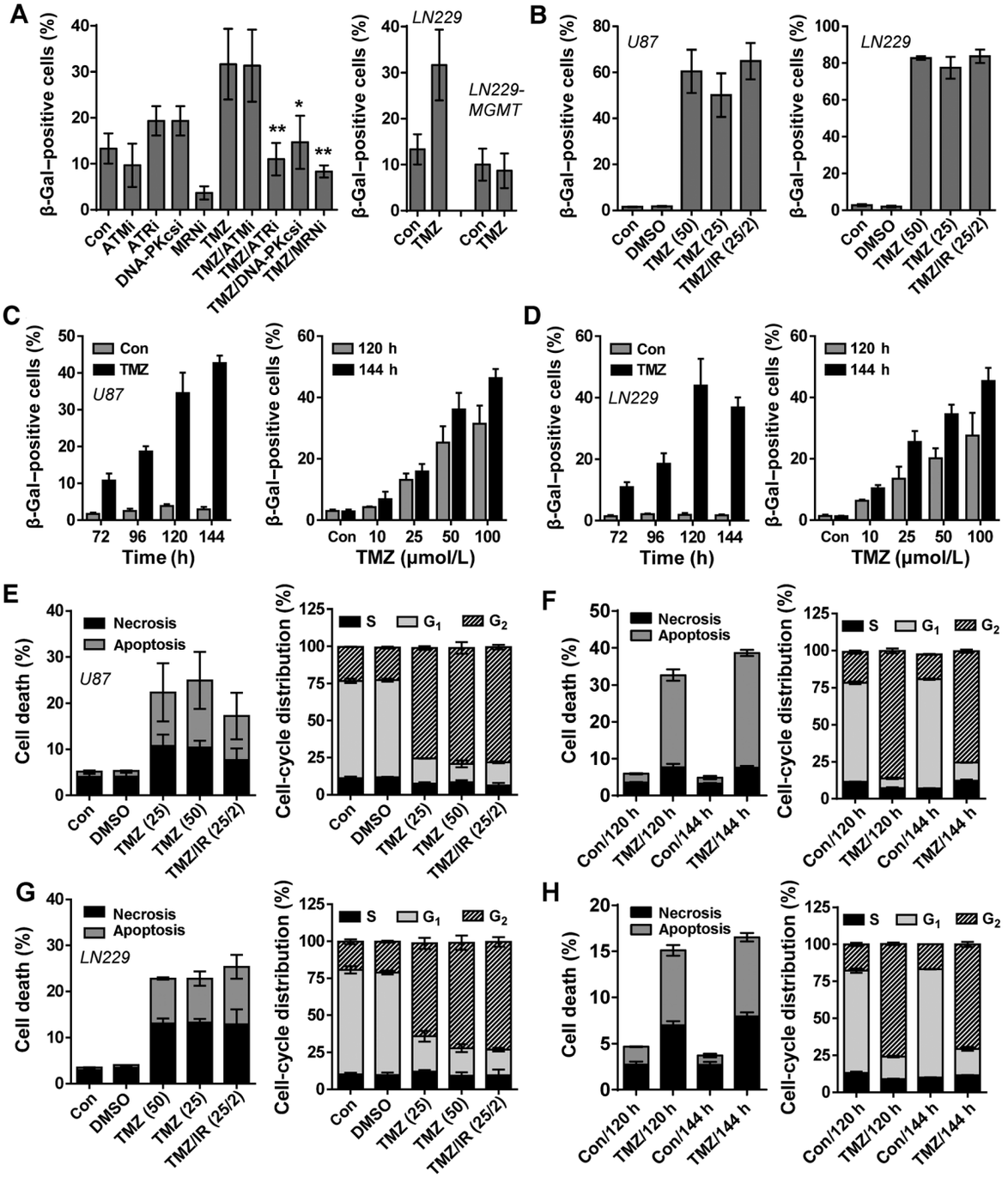

Figure 1.

A–D, Senescence was measured microscopically by detection of β-Gal–positive cells. **A,** LN229 cells were treated with inhibitors against ATR (ATR_i), ATM (ATM_i), DNA-PKcs ($DNA\text{-}PKcs_i$), and MRN (MRN_i). One hour later, cells were treated with 50 μmol/L temozolomide (TMZ) for 72 hours. In addition, also MGMT retransfected cells were treated with temozolomide. **B,** U87 and LN229 cells were nontreated or treated with temozolomide (25 or 50 μmol/L) or temozolomide (25 μmol/L)/IR (2 Gy) at 5 consecutive days; senescence was measured at day 8. U87 (**C**) and LN229 (**D**) cells were treated with 50 μmol/L temozolomide for different time points (left) or with different temozolomide concentrations for 120 and 144 hours (right). **E–H,** Cell death was measured by flow cytometry using Annexin V/PI staining (left) and cell-cycle distribution using PI staining (right). U87 (**E**) and LN229 (**G**) cells were nontreated or treated with temozolomide (25 or 50 μmol/L) or temozolomide (25 μmol/L)/IR (2 Gy) at 5 consecutive days; measurment occurred at day 8. U87 (**F**) and LN229 (**H**) cells were treated with 50 μmol/L temozolomide for 120 and 144 hours. **A–H,** Experiments were repeated at least three times; mean values ± SD are shown. In **A**, differences between temozolomide treatment and temozolomide/inhibitor treatment were statistically analyzed using Student *t* test (*, $P < 0.05$; **, $P < 0.01$).

LN229 (up to 80%) cells (Fig. 1B). Importantly, IR exposure did not influence senescence induction by temozolomide. Senescence was also activated upon single temozolomide exposure in a dose- and time-dependent manner, starting 72 hours after treatment with 25 μmol/L temozolomide in U87 (Fig. 1C) and LN229 cells (Fig. 1D), reaching 40% to 50% after 144 hours following exposure to 100 μmol/L temozolomide.

Compared with the high level of senescence, apoptosis and necrosis were induced at low levels (up to 20%) upon repeated treatment of U87 (Fig. 1E) and up to 10% necrosis and 25% apoptosis upon single exposure (Fig. 1F). Also, in LN229 cells repeated treatment induced up to 20% apoptosis and necrosis (Fig. 1G) and single exposure induced up to 15% apoptosis and necrosis (Fig. 1H).

The data indicate that senescence (as determined by β-Gal positivity) is the major endpoint induced by temozolomide followed by activation of cell death pathways. Of note, the strong activation of senescence by temozolomide was not affected by increased FCS-dependent proliferation stimuli because temozolomide induced a comparable frequency of senescence (as well as necrosis and apoptosis) in cells cultivated in 10% or 1% serum (Supplementary Fig. S1A–S1C). Because both chronic (Fig. 1E and G) and single exposure (Fig. 1F and H) induced a strong G_2–M arrest (>75%), we infer that temozolomide-induced senescence occurs in the G_2–M cell-cycle phase, which was also supported by the complete G_2–M-arrest observed in FACS-isolated senescent cells (see below).

Temozolomide-induced senescence is dependent on p21

An important pathway in activating cell-cycle arrest and senescence was shown to be triggered by p53-mediated induction of p21. The p53 wt glioma cell lines used in this study display a strong phosphorylation of p53 at Ser15 and the induction of p21 following temozolomide exposure (Fig. 2A). Contrary to U87 and LN229 cells, the p53-deficient LN308 and the p53-mutated U138 cells did not show p21 induction upon temozolomide exposure, neither on protein (Fig. 2B) nor on mRNA level (Fig. 2C). We should note that in p53-mutated U138 cells phosphorylation of p53 on Ser15 can be detected, which results, however, in a transcriptionally inactive protein. In line with the p53/p21 status, LN308 and U138 cells neither showed temozolomide-induced cell death (Supplementary Fig. S2A) nor senescence (Fig. 2D) in the dose range of up to 100 μmol/L. Contrary to senescence, the temozolomide-induced G_2–M arrest was independent of p53 and p21 (Fig. 2E). This suggests that upon temozolomide treatment, senescence, but not the G_2–M arrest, is dependent on p21. In line with this, knockdown of p21 (Supplementary Fig. S2B) completely abrogated the induction of senescence (Fig. 2F), but did not abrogate the G_2–M arrest (Fig. 2G).

Temozolomide-induced G_2–M arrest results from CHK1-dependent CDC25c degradation

The G_2–M transition is regulated by the CDK1/cyclin B complex. During the G_2 phase of the cell cycle, CDK1 is maintained in an inactive state due to WEE1-dependent phosphorylation at Tyr15. Activation of the CDK1/cyclin B complex and entry into mitosis is mediated via CDC25c-mediated Tyr15 dephosphorylation and CDK-activating kinase (CAK)–mediated phosphorylation at Thr161. Concerning the DNA damage–induced G_2–M arrest, it has been shown that CHK1 can phosphorylate CDC25c at Ser216, leading to nuclear export of CDC25c (23). It has also been shown that doxorubicin, camptothecin, and topotecan can induce a G_2–M arrest via CHK1-dependent CDC25a degradation (24, 25). We observed in U87 and LN229 cells a strong phosphorylation of CHK1 and CHK2 48 to 96 hours after temozolomide treatment (Fig. 3A). In parallel, a significant reduction in CDC25c protein (Fig. 3A) and an accumulation of cells in the G_2–M phase was observed (Supplementary Fig. S2C), while CDC25a remained unchanged. In line with the degradation of CDC25c, CDK1 remained inactive, as indicated by the missing (U87) or weak (LN229) dephosphorylation of CDK1 at Tyr15 (Supplementary Fig. S2D). Finally, a strong nuclear retention of the cyclin B1 complex was observed, further showing that the CDK1/cyclin B1 complex is kept in an inactive state (Supplementary Fig. S2E).

To elucidate whether CHK1 and CHK2 are responsible for the reduced expression of CDC25c and the activation of the G_2–M arrest, both factors were pharmacologically inhibited. Whereas inhibition of CHK1 counteracted the reduction in CDC25c protein (Fig. 3B) and prevented the G_2–M arrest (Fig. 3C), inhibition of CHK2 and p21 did not affect CDC25c protein level and only caused a minor reduction in the G_2–M arrest (Fig. 3C). Vice versa, inhibition of p21 and, to a lesser extent, CHK1, but not CHK2, abrogated senescence (Fig. 3D). Similar results were obtained using a second CHK1 inhibitor and CHK1-specific siRNA (Supplementary Fig. S3A–S3D). To address the impact of the initial DDR kinases on the G_2–M arrest, ATM, ATR, MRN, and DNA-PK_{cs} were inhibited and the cell-cycle distribution was measured in LN229 cells (Fig. 3E). The data show, that similar to senescence, the G_2–M arrest is dependent on ATR, but not ATM. Interestingly, in this case, inhibition of MRN and DNA-PKcs did not prevent the G_2–M arrest. Because MGMT-expressing cells did not display a G_2–M arrest, it is obvious that the observed cell-cycle arrest is triggered by the specific DNA lesion O^6MeG.

Maintenance of temozolomide-induced senescence is mediated through NF-κB

Senescence can be divided into two phases, initiation and maintenance (26). To render senescence irreversible, further cellular changes have to occur. During the maintenance phase, the cell-cycle arrest becomes irreversible (13), mainly through the accumulation of p14 and p16. Furthermore, it was reported that either p14 or p16 or both can take over the role of p21 in maintaining senescence. In this context, it is important to note that up to 50% of gliomas show a deletion of p14/16 (27). Among the cell lines used in our study, U87, U138, and LN229 harbor a deletion in exon 1 of CDKN2A as indicated by methylation-specific PCR (MSP) detecting both the unmethylated and the methylated exon 1 (Supplementary Fig. S4A and S4B) and show no *p14/p16* mRNA expression (Supplementary Fig. S4C), whereas LN308 cells are p14/p16 proficient. Interestingly, LN308 cells do not show temozolomide-induced senescence, which is not supporting the view that p14/p16 can substitute for p21, at least in the process that leads to temozolomide-induced senescence of glioma cells.

Other mechanisms maintaining senescence were reported to depend on an NF-κB-dependent amplifying loop, leading to enhanced ROS production (28). To analyze the impact of NF-κB on temozolomide-induced senescence, expression of the NF-κB inhibitor IκB was analyzed (Fig. 4A). IκB protein level was strongly reduced 48 hours after temozolomide in U87 and LN229 cells, indicating activation of NF-κB. This was further supported by reporter assays showing enhanced NF-κB activity upon

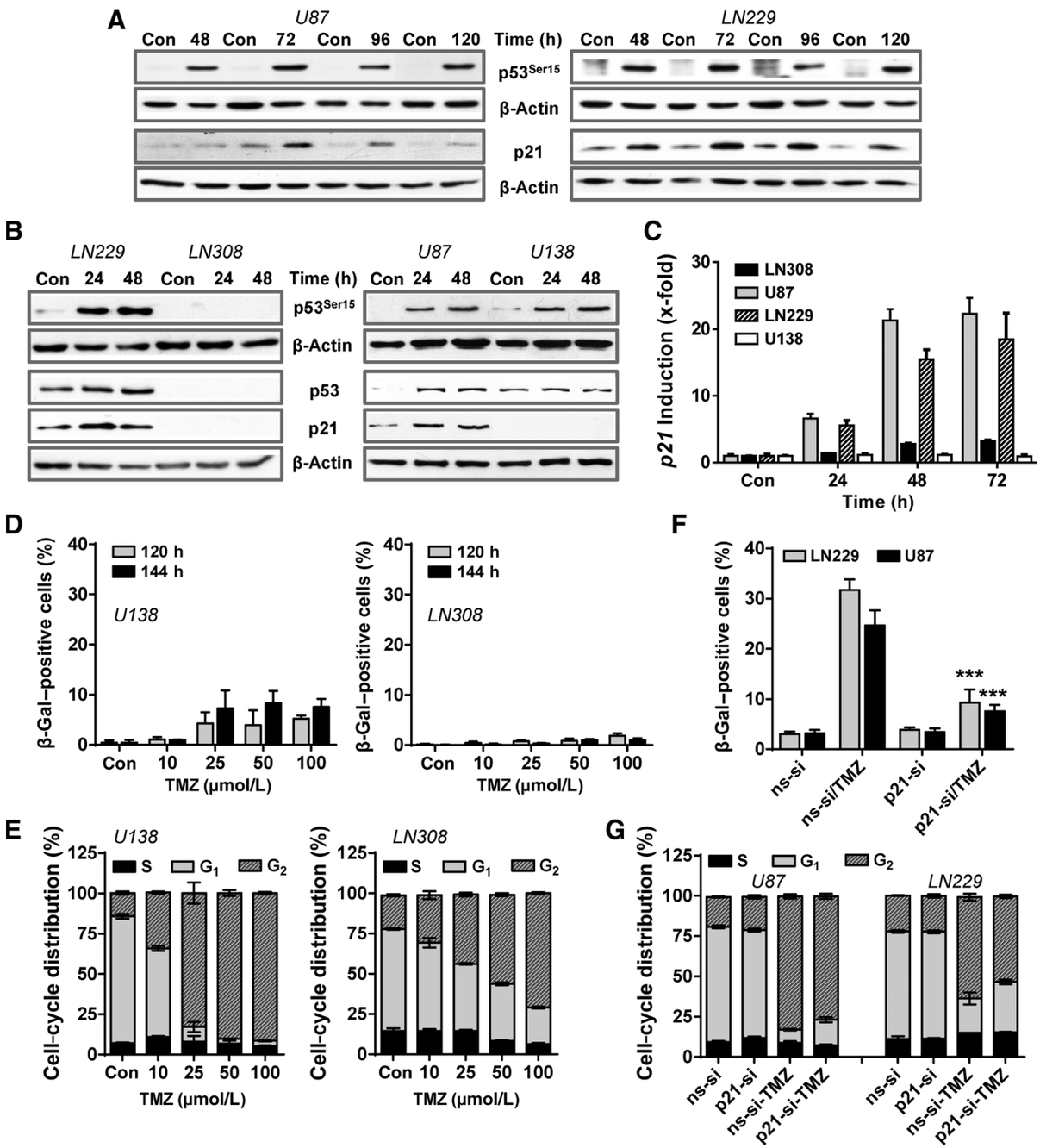

Figure 2.

A, p53 phosphorylation at Ser[15] and p21 expression was determined by immunoblotting 48 to 120 hours after temozolomide (100 μmol/L) exposure in U87 (left) and LN229 (right) cells. Con, untreated cells. β-Actin was used as internal loading control. **B,** p53 phosphorylation at Ser[15], as well as p53 and p21 expression, was determined by immunoblotting 24 to 48 hours after temozolomide (100 μmol/L) exposure in LN229, LN308, U87, and U138 cells. **C,** *p21* mRNA expression was measured by qRT-PCR 24 to 72 hours after temozolomide (100 μmol/L) exposure in LN229, LN308, U87, and U138 cells. **D,** Concentration-dependent induction of senescence was measured by detection of β-Gal–positive cells 120 and 144 hours after temozolomide (TMZ) exposure in U138 and LN308 cells. **E,** Cell-cycle distribution was measured using PI staining and flow cytometry 120 hours after temozolomide exposure in U138 and LN308 cells. **F** and **G,** LN229 and U87 cells were transfected with nonsilencing siRNA (ns-si) and p21-specific siRNA (p21-si). Sixteen hours later, cells were treated with 100 μmol/L temozolomide. After 120 hours, senescence was measured by detection of β-Gal–positive cells (**F**) and cell-cycle distribution was measured using PI staining and flow cytometry (**G**). **A–G,** Experiments were repeated at least three times; mean values ± SD are shown. In **F**, differences between temozolomide/ns-si treatment and temozolomide/p21-si treatment were statistically analyzed using Student *t* test (***, $P < 0.001$).

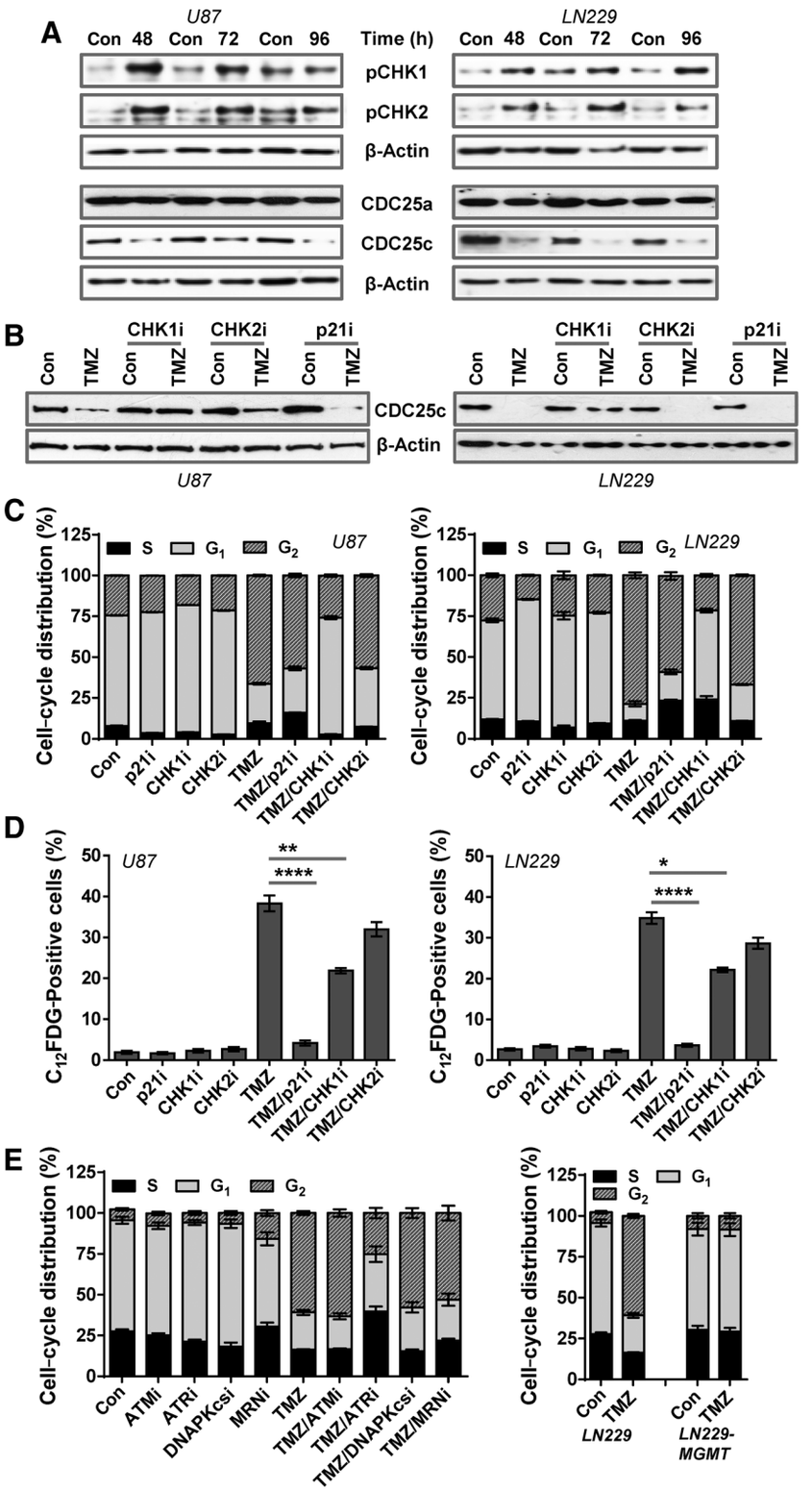

Figure 3.

A, Phosphorylation of CHK1 and CHK2, as well as expression of CDC25a and CDC25c, was determined by immunoblotting 48 to 96 hours after temozolomide (100 μmol/L) exposure in U87 (left) and LN229 (right) cells. **B–D,** U87 and LN229 cells were treated with inhibitors against CHK1 (UCN-01 = $CHK1_i$), CHK2 ($CHK2_i$), and p21 (UC2288 = $p21_i$) and 1 hour later with 100 μmol/L temozolomide (TMZ). **B,** Expression of CDC25c was determined by immunoblotting 72 hours upon temozolomide exposure. **C,** Cell-cycle distribution was measured using PI staining and flow cytometry 72 hours after temozolomide exposure. **D,** Induction of senescence was measured by FACS-based detection of C_{12}FDG-positive cells 120 hours after temozolomide exposure. Differences between temozolomide treatment and temozolomide/inhibitor treatment were statistically analyzed using Student *t* test (*, $P < 0.05$; ****, $P < 0.0001$). **E,** LN229 cells were treated with inhibitors against ATR (VE-821 = ATR_i), ATM (KU60019 = ATM_i), DNA-PKcs (KU0060648 = $DNA\text{-}PKcs_i$), and MRN (Mirin = MRN_i). One hour later, cells were treated with 50 μmol/L temozolomide for 72 hours and cell-cycle distribution was measured. In addition, MGMT-retransfected cells were also treated with temozolomide. **C–E,** Experiments were repeated at least three times; mean values ± SD are shown.

temozolomide exposure (Supplementary Fig. S5A). A clinically relevant mechanism triggered by NF-κB is the senescence-associated secretory phenotype (SASP), which is characterized by the induction and secretion of different cytokines (29). To analyze whether temozolomide can induce SASP, the time-dependent expression of the inflammatory cytokines IL6 and IL8, which are

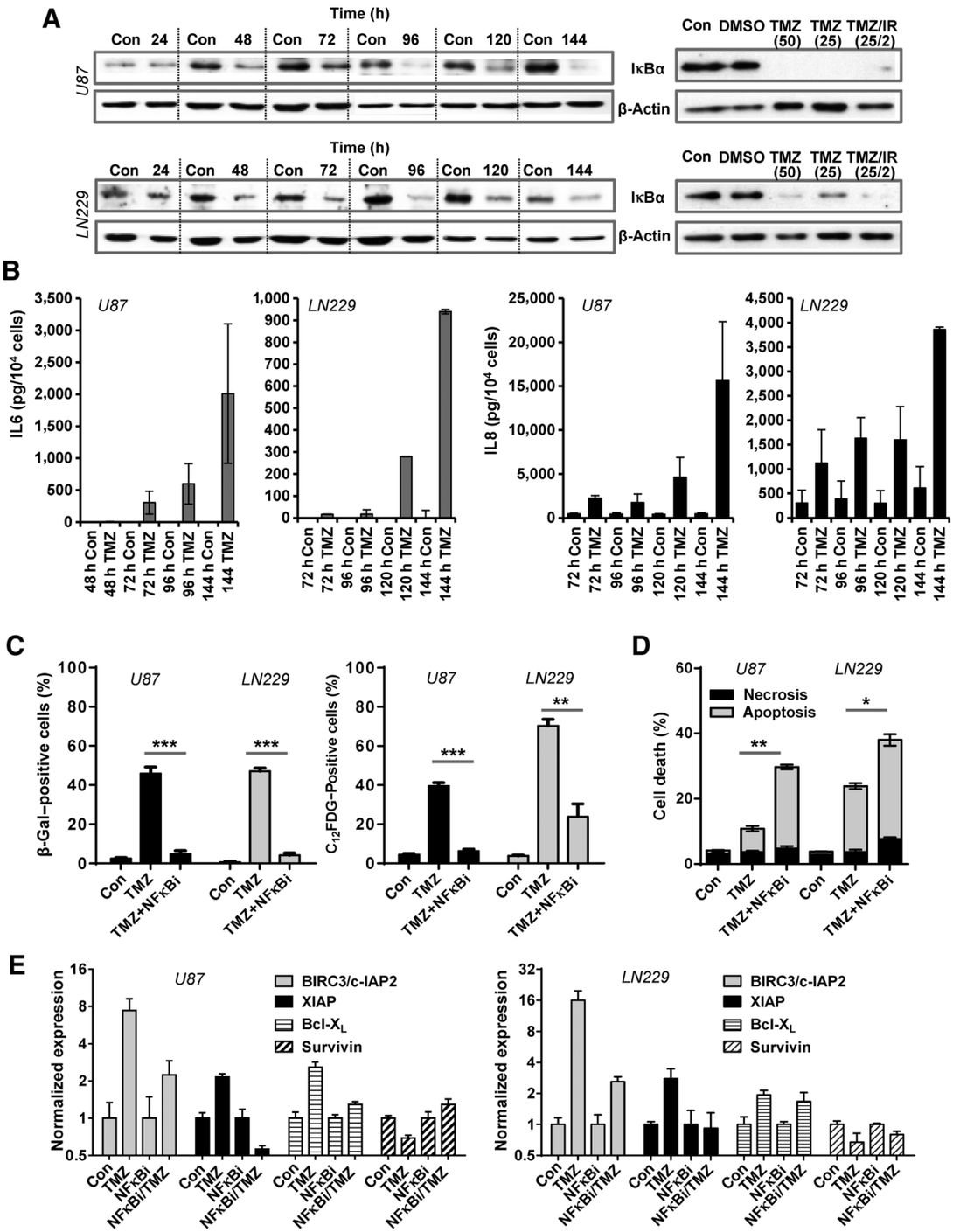

Figure 4.

A, LN229 and U87 cells were treated with 100 μmol/L temozolomide (TMZ) for different time points (left) or cells were nontreated or treated with temozolomide (25 or 50 μmol/L) or temozolomide (25 μmol/L)/IR (2 Gy) at 5 consecutive days; protein isolation occurred at day 8 (right). Expression of IκB was determined by immunoblotting. **B,** U87 and LN229 cells were treated with 100 μmol/L temozolomide for different time points. Secretion of IL6 and IL8 was measured by ELISA. **C** and **D,** U87 and LN229 cells were treated with 50 μmol/L temozolomide and 48 hours later with the NF-κB inhibitor III. **C,** Senescence was measured 144 hours upon temozolomide exposure via β-Gal staining and flow cytometry–based acquisition of C_{12}FDG-positive cells. **D,** Cell death was measured using Annexin V/PI staining and flow cytometry. **B–D,** Experiments were repeated at least three times; mean values ± SD are shown. **C–D,** Differences between temozolomide treatment and temozolomide/inhibitor treatment were statistically analyzed using Student *t* test (*, $P < 0.05$; **, $P < 0.01$; ***, $P < 0.001$). **E,** U87 and LN229 cells treated with 100 μmol/L temozolomide in the presence or absence of NF-κB inhibitor III. Seventy-two hours later, expression of *c-IAP2, XIAP, BCL-X$_L$*, and *Survivin* mRNA was measured by qRT-PCR.

main components of SASP, were analyzed in U87 and LN229 cells. The data clearly show that temozolomide induces the expression of *IL6*/*IL8* mRNA (Supplementary Fig. S5B) and augments the production of IL6 and IL8 in glioma cells (Fig. 4B). To investigate the role of NF-κB in temozolomide-induced senescence, NF-κB was pharmacologically inhibited. The inhibitor was added for 48 hours and senescence was analyzed 144 hours after temozolomide exposure via β-Gal staining and flow cytometry–based measurement of C_{12}FDG-positive cells (Fig. 4C). For verification, the experiments were repeated using an alternative NF-κB inhibitor (Supplementary Fig. S5C). The results showed a dramatic reduction in temozolomide-induced senescence following NF-κB inhibition (Fig. 4C). Interestingly, these experiments also revealed an increase in apoptosis (Fig. 4D), indicating that NF-κB might be important in triggering the switch between temozolomide-induced senescence and apoptosis. To analyze the impact of NF-κB on the expression of antiapoptotic factors, the expression of *c-IAP2*, *Bcl-X_L*, *Survivin*, and *XIAP*, known transcriptional targets of NF-κB, were determined. The data indicate a strong time-dependent induction of *c-IAP2* and a weak induction of *Bcl-X_L* and *XIAP* (Supplementary Fig. S5D). *Survivin* expression was not induced. Induction of *c-IAP2* and *Bcl-X_L* was significantly reduced by NF-κB inhibition (Fig. 4E), suggesting that these factors are involved in apoptosis prevention upon temozolomide exposure.

Temozolomide induces senescence-associated transcriptional repression of DNA repair factors

To elucidate whether temozolomide-induced senescence alters the cellular DNA repair capacity, we analyzed the expression of various DNA repair factors involved in the resistance against temozolomide on RNA level. Thus, we observed that several DNA repair genes, including the MMR genes *EXO1*, *MSH2*, *MSH6*, and an important component of HR, namely *RAD51*, are transcriptionally repressed following temozolomide exposure. All four genes showed reduced expression starting 48 hours after exposure to 100 μmol/L temozolomide in LN229 and U87 cells (Fig. 5A), whereas the p53 target gene *DDB2* was upregulated. Next, we analyzed the impact of transcriptional repression on the corresponding proteins. The data show that reduced transcription resulted in decreased MSH2, MSH6, EXO1, and RAD51 protein expression, both following single (Fig. 5B) and repeated temozolomide exposure (Fig. 5C). The reduced mRNA and protein levels had an impact on the cellular repair capacity, as shown by decreased MMR-binding activity (Fig. 5D) and reduced HR activity (Fig. 5E) upon temozolomide treatment.

Temozolomide-induced transcriptional repression of *EXO1*, *MSH2*, *MSH6*, and *RAD51* is mediated by decreased E2F1/DP1 signaling

Because ChIP-Seq and ChIP-chip studies have described *EXO1*, *MSH2*, *MSH6*, and *RAD51* as potential targets of E2F1 and E2F4 (30, 31), we analyzed the role of E2F1 in the repression of EXO1, MSH2, MSH6, and RAD51. Thus, we measured the expression of E2F1 and its binding partners DP1 and RB as well as E2F1 phosphorylation on protein level upon single and chronic temozolomide exposure. The data (shown in Supplementary Fig. S6A–S6D) revealed only minor alterations in the overall protein levels of E2F1, DP1, and RB. Only upon chronic exposure of U87 cells, a decrease of DP1 protein was observed. Similarly, the phosphorylation of E2F1 at Ser^{337} (target of CDK4/6, enhancing transcriptional activity) and Ser^{364} (target of CHK2) was not altered upon temozolomide exposure.

Because the activity of E2F1 strongly depends on its interaction with DP1, we analyzed the complex formation between E2F1 and DP1 via coimmunoprecipitation. The results clearly show that the complex between E2F1 and DP1 was disrupted by temozolomide, both upon single and chronic exposure (Fig. 6A and B). Finally, we analyzed the binding of E2F1 and DP1 to the promoter of *EXO1*, *MSH2*, *MSH6*, and *RAD51* using ChIP. Binding of E2F1 (Fig. 6C), and even more pronounced of DP1 (Fig. 6D) to the corresponding promoters was strongly reduced 48 hours and 72 hours following temozolomide exposure, indicating that these genes are silenced because of lack of activation by E2F1/DP1.

Next, we addressed the question of whether gene silencing is a direct response to the G_2–M arrest or whether it is associated with senescence. As shown in Fig. 2, U138 and LN308 showed a strong G_2–M arrest without inducing senescence. Despite the G_2–M arrest, these cells showed no reduction in the expression of *EXO1*, *MSH2*, *MSH6*, or *RAD51* (Supplementary Fig. S6E), indicating that the repression is not directly caused by the G_2–M arrest, but might be associated with the p21-induced senescence phenotype. This assumption was supported by the finding that siRNA-mediated knockdown of p21 did not only prevent senescence, but also abrogated the repression of *EXO1*, *MSH2*, *MSH6*, and *RAD51* (Fig. 6E).

Temozolomide-induced transcriptional repression of EXO1, MSH2, MSH6, and RAD51 occurs in senescent cells

To further support the hypothesis that the temozolomide-induced repression of EXO1, MSH2, MSH6, and RAD51 is a specific feature of senescent cells, temozolomide-induced senescent cells were separated by flow cytometry using C_{12}FDG for labeling. The frequency of senescence in the sorted cells as well as in unsorted cells exposed or not exposed to temozolomide was verified microscopically by β-Gal staining, showing that the FACS-enriched cell population contained appoximately 95% senescent cells (Fig. 7A and B, left). Moreover, cell-cycle distribution was measured, revealing that approximately 90% of the C_{12}FDG-isolated senescent cells were arrested in the G_2–M phase of the cell cycle (Fig. 7A and B, middle), clearly showing that temozolomide-induced senescent cells are arrested in the G_2–M phase. Finally, the expression of EXO1, MSH2, MSH6, and RAD51 was analyzed in C_{12}FDG-sorted cells. The data show strongly reduced protein levels of these proteins in the senescent population (Fig. 7A and B, right).

Repression of EXO1, MSH2, MSH6, and RAD51 in mouse xenografts treated with temozolomide

To determine whether temozolomide also reduces the expression of EXO1, MSH2, MSH6, and RAD51 in glioma cells grown in a host *in vivo*, U87 cells were injected into immunodeficient mice. As shown in Fig. 7C, temozolomide treatment of mice clearly reduced EXO1, MSH2, MSH6, and RAD51 protein, as well as CDC25c protein level. Furthermore, the protein level of IκB decreased and the level of p21 increased following systemic temozolomide treatment. Thus, the same phenotype was observed *in vivo*, supporting the notion that temozolomide has the potency to trigger senescence in tumors, which is accompanied by downregulation of the repair pathways referred to above.

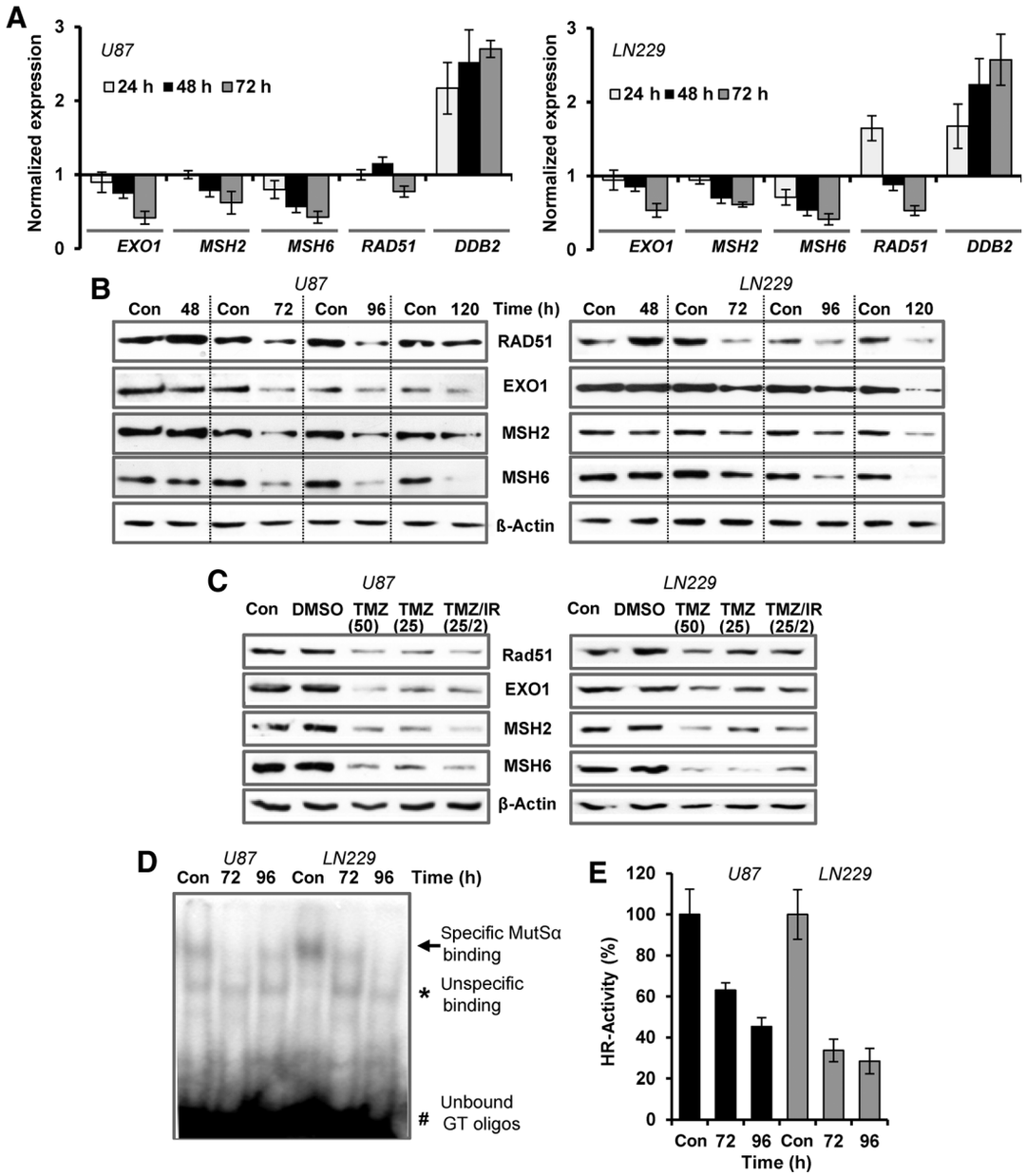

Figure 5.

A, Time-dependent expression of *EXO1, MSH2, MSH6, RAD51, and DDB2* was determined by qRT-PCR after temozolomide (100 μmol/L) exposure in U87 and LN229 cells. Expression was normalized to gapdh and β-actin; the untreated control was set to one. **B,** Time-dependent expression of EXO1, MSH2, MSH6, and RAD51 protein was determined after temozolomide (100 μmol/L) exposure by immunoblotting in U87 and LN229 cells. β-Actin was used as internal loading control. **C,** U87 and LN229 cells were nontreated or treated with temozolomide (TMZ, 25 or 50 μmol/L) or temozolomide (25 μmol/L)/IR (2 Gy) at 5 consecutive days; protein isolation occurred at day 8. Expression of EXO1, MSH2, MSH6, and RAD51 was determined by immunoblotting. β-Actin was used as internal loading control. **D** and **E,** U87 and LN229 cells were treated with 100 μmol/L temozolomide for 72 and 96 hours. **D,** MSH2/MSH6-binding activity was analyzed by EMSA. **E,** HR activity was analyzed using the PCR-based HR Assay Kit from Norgen Biotec Corp. ID 35600.

Discussion

The therapy of high-grade gliomas rests on treatment with the anticancer drug temozolomide, which is highly effective in inducing apoptosis (9). However, at treatment-relevant doses not all cells are killed by apoptosis, which is likely the reason why temozolomide treatment can only extend the median survival of patients from 12.1 to 14.6 months (6). Activation of apoptosis through temozolomide is triggered by the minor DNA lesion O^6MeG and subsequent activation of the DDR (22). Using synchronized cells, we further showed that O^6MeG triggers the accumulation of cells in the G_2–M phase of the posttreatment cell cycle (32). Besides inducing cell death through apoptosis,

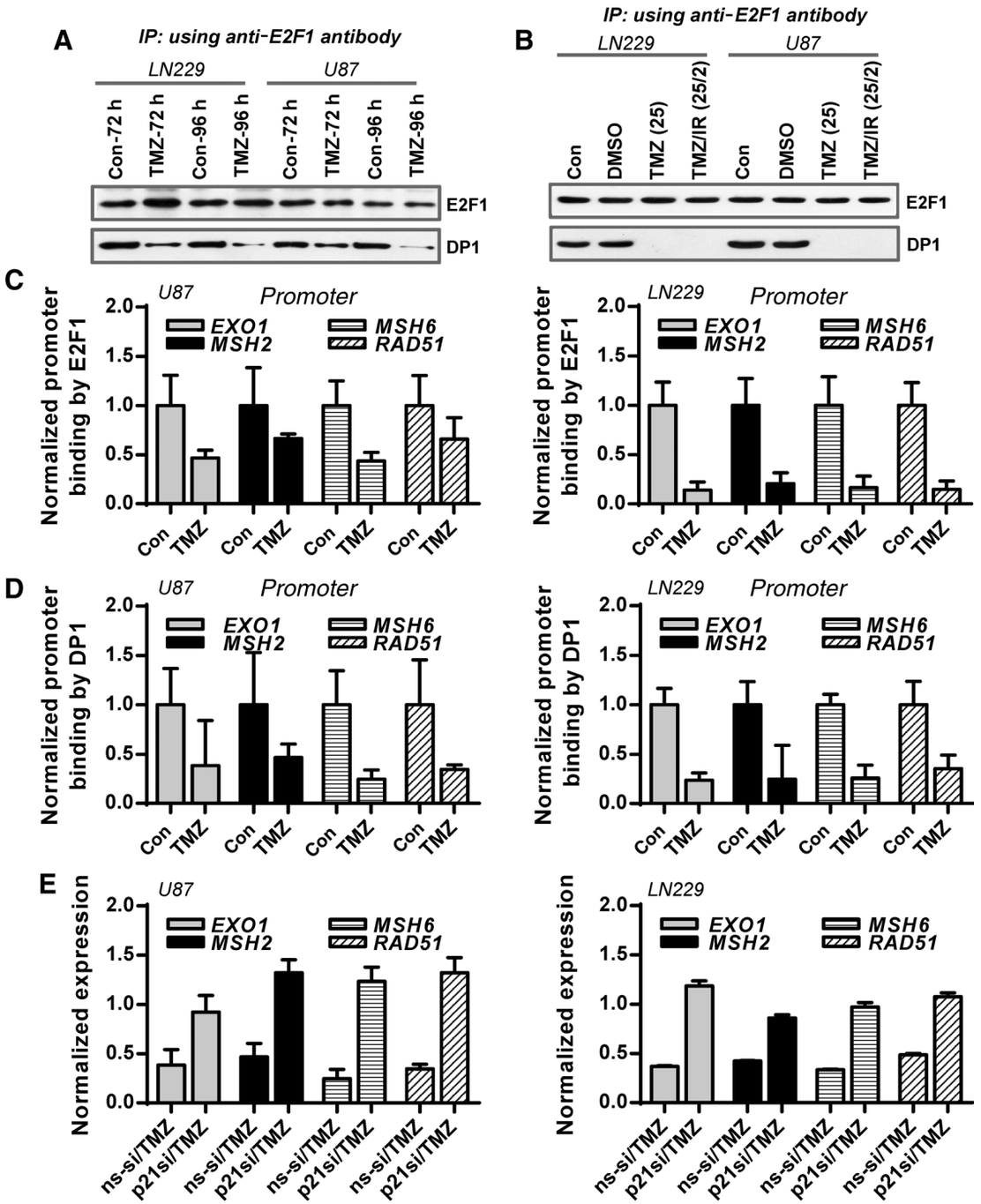

Figure 6.

A, LN229 and U87 cells were treated with 100 μmol/L temozolomide (TMZ) for 72 and 96 hours. **B,** LN229 cells and U87 cells were nontreated or treated with temozolomide (25 or 50 μmol/L) or temozolomide (25 μmol/L)/IR (2 Gy) at 5 consecutive days; protein isolation occurred at day 8 (right). **A** and **B,** Whole-cell extracts were prepared and E2F1 was immunoprecipitated (IP) using specific antibody against E2F1. Fifty percent of the immunoprecipitated proteins were separated by SDS-PAGE and E2F1 was detected by immunodetection. Fifty percent of the immunoprecipitated proteins were separated by SDS-PAGE and DP1 was detected by immunodetection. **C** and **D,** ChIP analysis was performed in U87 and LN229 cells 72 hours after exposure to 100 μmol/L temozolomide. Protein–DNA complexes were immunoprecipitated with anti-E2F1 (**C**) or anti-DP1 (**D**) antibody and qRT-PCR was performed using primers flanking the E2F1-responsive element within the *EXO1, MSH2, MSH6,* and *RAD51* promoter. **E,** U87 and LN229 cells were transfected with nonsilencing siRNA (ns-si) and p21-specific siRNA (p21si). Twenty-four hours later, cells were treated with 100 μmol/L temozolomide and 72 hours later the expression of *EXO1, MSH2, MSH6,* and *RAD51* mRNA was measured by qRT-PCR.

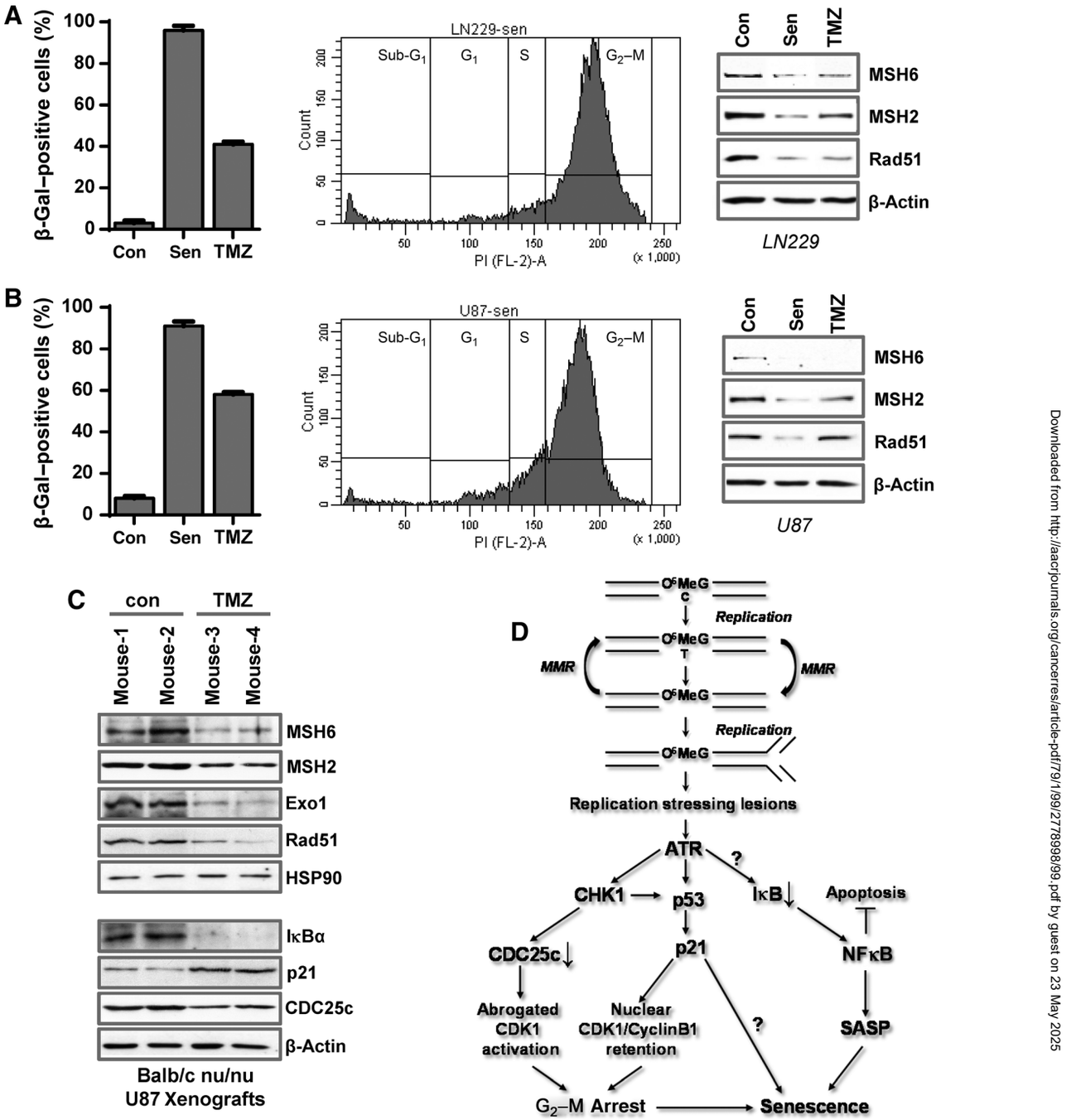

Figure 7.

LN229 (**A**) and U87 (**B**) cells were nontreated (Con) or treated with 100 μmol/L temozolomide (TMZ) for 120 hours. In parallel, cells were treated with 100 μmol/L temozolomide for 120 hours and C_{12}FDG-positive cells were separated by FACS (Sen). Senescence was verified via β-Gal staining (left) and cell-cycle distribution was measured using PI staining (middle). Whole-cell extracts were prepared and EXO1, MSH2, MSH6, and RAD51 were detected by immunodetection (right). β-Actin was used as internal loading control. **C,** U87 cells were injected into immunodeficient (Balb/c nu/nu) mice. Upon tumor formation, the mice were either mock treated or treated with temozolomide (200 mg/kg body weight in DMSO/NaCl i.p.). Ninety-six hours later, mice were sacrificed and the tumors isolated. For analysis the left and right tumors were combined and protein expression of various proteins was determined by immunoblotting. **D,** Model summarizing temozolomide-induced senescence. Upon temozolomide exposure, the initial damage O^6MeG is processed into replication stressing lesions via futile MMR cycles, leading to the activation of the DDR. ATR activates CHK1, which targets CDC25c for degradation, leading to abrogated CDK1 activation and G_2–M arrest. In parallel, the DDR activates p53, leading to the expression of p21, which causes nuclear retention of the inactive CDK1/cyclin B1 complex, thereby prolonging the G_2–M arrest. We suppose that other, unknown functions of p21 are additionally required for the induction and maintenance of senescence. Furthermore, degradation of IκB and, thereby, activation of NF-κB is required for temozolomide-induced senescence through induction of the SASP, which maintains senescence or by prevention of apoptosis.

temozolomide also activates survival pathways such as DNA repair, autophagy, and senescence (2). Comparing the data quantitatively, it appears that apoptosis is only a minor pathway, whereas senescence represents a dominant trait triggered by temozolomide in glioblastoma cells.

Hallmarks of cellular senescence are activation of the DDR and subsequent induction of a cell-cycle arrest. During replicative and oncogenic senescence as well as following exposure to many genotoxic agents, senescent cells are arrested in the G_1 phase. This is in contrast to our finding that temozolomide induces senescence in the G_2–M phase. Data concerning the activation of senescence in the G_2 phase of the cell cycle are limited (33). In normal human cells, the G_2–M arrest and subsequent senescence were analyzed following treatment with the topoisomerase II inhibitor ICRF-193. In this system, the G_2–M arrest depends on p21, which was associated with nuclear retention of cyclin B1, as well as with the accumulation of RB (34). Furthermore, p21 has also been shown to sequester inactive cyclin B1–Cdk1 complexes in the nucleus of ICRF-193–exposed human fibroblasts (35–37). In contrast to this, in human HCT-116 or U2OS cancer cells, no nuclear retention of cyclin B1 was observed during DNA damage–induced G_2–M arrest (38). The discrepancy between normal and cancer cells was explained by the fact that HCT-116 or U2OS cells, despite being p53-proficient, show inefficient and late p21 activation after treatment with ICRF-194 or the radiomimetic drug bleomycin (39).

According to our study, both the activation of the G_2–M arrest and the senescence is triggered by the specific DNA damage O^6MeG. It is important to note that induction of the G_2–M arrest occurs in both p53-proficient and p53-deficient cells. The G_2–M arrest was completely abrogated upon inhibition of CHK1, but not p21, clearly indicating that induction of the G_2–M arrest in temozolomide-exposed glioma cells is independent of p21. According to our findings, activation of the temozolomide-induced G_2–M arrest occurs through the CHK1-dependent degradation of CDC25c and the subsequent lack of CDK1 activation. This is in line with a report showing that dysfunctional telomeres activate DDR and promote CHK1/CHK2–dependent phosphorylation of CDC25c at Ser216, leading to its proteasomal degradation and the induction of the G_2–M arrest (40). In contrast to the G_2–M block induced by dysfunctional telomeres, the temozolomide-induced G_2–M arrest appears to depend only on ATR and CHK1 and not on ATM and CHK2. Furthermore, our findings confirm data that highlight the importance of CHK1 activation for inducing the temozolomide-induced G_2–M arrest in glioma cells (3, 4).

Upon activation of the G_2–M arrest, p21 appears to be crucial for rendering the cell-cycle arrest irreversible and activating the senescent phenotype. The exact mechanism by which p21 induces temozolomide-induced senescence is, however, still unclear. Contrary to data obtained in HCT-116 or U2OS cancer cells (38, 39), we observed a strong and long-lasting nuclear retention of cyclin B1 after temozolomide treatment, suggesting that p21-dependent sequestration of inactive cyclin B1–CDK1 complexes may be important for p21-mediated endurance of the temozolomide-induced G_2–M arrest and senescence. Besides p21, also NF-κB signaling is important for temozolomide-induced senescence. Thus, we provide evidence that temozolomide treatment leads to the degradation of the NF-κB inhibitor IκB, which results in activation of NF-κB and the upregulation of NF-κB targets such as IL6 and IL8. Interestingly, we observed that inhibition of NF-κB abrogates senescence and shifts cells into apoptosis. In parallel, a strong induction of the antiapototic NF-κB target BIRC3/c-IAP2 was observed after temozolomide treatment. Because BIRC3/c-IAP2 induction was abrogated by NF-κB inhibition, we suppose that this factor might be causally involved in the protection against temozolomide-induced apoptosis. This is in line with data showing that BIRC3/c-IAP2 upregulation results in apoptosis evasion and therapeutic resistance of glioblastoma (41). Altogether, our data suggest that NF-κB supports senescence by activation of SASP, which is thought to maintain senescence, and/or NF-κB-dependent activation of antiapoptotic factors and thereby abrogation of cell death.

Studying the DNA repair status in temozolomide-induced senescent cells, we observed that the MMR genes *EXO1*, *MSH2*, *MSH6*, and the rate-limiting factor of HR, *RAD51*, are transcriptionally repressed. This was accompanied by low-level expression of the corresponding proteins and diminished DNA repair capacity. As indicated by immunoprecipitation and ChIP experiments, repression of these genes was caused by the disruption of the E2F1/DP1 complex. The data showing E2F1-dependent regulation of MSH2 and MSH6 are in line with the previous observation that E2F1 can regulate MSH2 and MSH6 in rat cells (42). They are also compatible with the finding that embryonal stem cells of mice show a higher expression of MSH2 and MSH6 compared with differentiated cells due to increased E2F1 activity (43). Corresponding to the fact that MMR and HR are needed in S/G2, a higher expression of MSH2 and RAD51 has been described in these cell-cycle phases (44). Here, we describe for the first time a nearly complete repression of these factors and, in addition to these, of MSH6 and EXO1 upon genotoxic stress. The transcriptional repression in temozolomide-treated glioma cells is not caused by an arrest in G_0–G_1 and also not by accumulation of cells in G_2–M per se, because the repression of these repair proteins cannot be observed in G_2–M-arrested p53-deficient cells in the absence of p21. The repression strongly depends on the induction of p21-mediated senescence. The finding that senescent cells isolated by FACS showed strongly reduced expression of *EXO1*, *MSH2*, *MSH6*, and *RAD51* supports the idea that repression of these repair factors is part of the SASP.

We are aware of the fact that nonreplicating senescent glioma cells are necessarily refractory to killing by temozolomide, because O^6MeG adducts need replication to be converted into DSBs (7). Therefore, the downregulation of repair proteins has presumably no direct impact on temozolomide resistance. However, we consider the possibility that as a result of impaired DNA repair capacity, including the HR pathway, DSBs induced by concomitant radiotherapy and other types of spontaneously arising DNA damage will not be repaired in an error-free way in senescent cells. This may lead to further genomic alterations, which could contribute to increased aggressiveness of recurrent tumors once senescent cells become reactivated. Can this happen?

Commonly, senescence is considered to be a clinically favorable response to chemotherapy because it is thought to permanently block the proliferation of tumor cells and, therefore, stop tumor growth. However, several studies provided hints that cells can escape from genotoxin-induced senescence (13–15). In addition, regrowth experiments following temozolomide treatment have been performed in U87 cells showing restart of growth one week after temozolomide exposure (45). However, these experiments could not prove convincingly regrowth of senescent cells. The question concerning reversibility of temozolomide-induced

senescence is therefore still open. It is of central importance and has to be urgently addressed in future experiments.

Another question that remains to be solved is whether the expression of *EXO1*, *MSH2*, *MSH6*, and *RAD51* recovers once glioma cells escape from senescence, or whether the long-lasting transcriptional repression results in epigenetic silencing via histone modifications or CpG methylation. The latter hypothesis gains support from the findings that reduced MMR activity was observed in melanomas after exposure to temozolomide (46) and significantly lower MLH1, MSH2, MSH6, and PMS2 protein levels were observed in recurrent glioblastomas (47, 48). Importantly, it was shown that the MSH2 and MSH6 levels are quantitatively related to the sensitivity of cells to methylating agents (49) and that even minor changes in the expression of MSH2 can have an impact on the response of gliomas to temozolomide (50). Another open issue pertains to the question of selective killing of senescent cells and drug-induced reactivation of senescent cells, considering the possibility of improving the efficacy of temozolomide. Some of these modifying drugs like resveratrol were shown to act via reinforcing the temozolomide-induced senescence in glioma cells (51). Opposite, selective killing of senescent cells using senolytic drugs (52) may also improve temozolomide-based therapy of malignant glioma. Thus, drug combinations targeting in a specific way both the senescence and the apoptosis pathway should be tested in future studies.

In summary, temozolomide induces senescence at high level in glioma cells. This scenario is outlined in Fig. 7D. The arrest in the G_2–M phase of the cell cycle is initiated via ATR/CHK1–mediated degradation of CDC25c leading to abrogated CDK1/cyclin B1 activity and is further fixed into senescence via p21. Furthermore, there is growing evidence that NF-κB is important for temozolomide-induced senescence. In this process, NF-κB could act by induction of antiapoptotic factors, thereby suppressing the apoptotic pathway and/or by induction of the SASP. Concomitant to senescence, a transcriptional repression of *EXO1*, *MSH2*, *MSH6*, and *RAD51* was observed, which is mediated by disruption of the E2F1/DP1 complex. Therefore, reduced MMR and HR capacity can be considered a specific phenotype of temozolomide-induced senescence, which could enhance the aggressiveness of these cells once they restart to replicate, by allowing additional mutational and genomic alterations. These alterations may facilitate tumor progression and contribute to the formation of therapy-resistant recurrences.

Disclosure of Potential Conflicts of Interest

No potential conflicts of interest were disclosed.

Authors' Contributions

Conception and design: D. Aasland, W.P. Roos, M.T. Tomicic, B. Kaina, M. Christmann
Development of methodology: D. Aasland, J. Meyer, M.T. Tomicic
Acquisition of data (provided animals, acquired and managed patients, provided facilities, etc.): D. Aasland, N. Berte, E.E. Reuber, M. Christmann
Analysis and interpretation of data (e.g., statistical analysis, biostatistics, computational analysis): D. Aasland, L. Hauck, J. Meyer, M. Effenberger, S. Schneider, W.P. Roos, M.T. Tomicic, B. Kaina, M. Christmann
Writing, review, and/or revision of the manuscript: D. Aasland, N. Berte, W.P. Roos, M.T. Tomicic, B. Kaina, M. Christmann
Administrative, technical, or material support (i.e., reporting or organizing data, constructing databases): D. Aasland, S. Schneider, M.T. Tomicic
Study supervision: M.T. Tomicic, B. Kaina, M. Christmann
Others (performing experiments): L. Götzinger, M. Effenberger
Others [assistance in practical research work (experiments and interpretation)]: L. Hauck
Others (shared senior/corresponding authorship): M.T. Tomicic, B. Kaina, M. Christmann

Acknowledgments

This study was funded by grants from the Wilhelm Sander Stiftung (AZ – 2014.102.1 to M. Christmann) and the German Science Foundation (DFG CH 665/6-1 to M. Christmann), by a grant of the German Cancer Aid (Mildred Scheel Foundation, AZ – 111404 to M.T. Tomicic and M. Christmann), and by a grant of the German Science Foundation (DFG KA724/18-1,2 to B. Kaina). We greatly appreciate the technical assistance of Birgit Rasenberger and support by Christian Schwarzenbach. Support by IMB's Flow Cytometry Core Facility is gratefully acknowledged.

The costs of publication of this article were defrayed in part by the payment of page charges. This article must therefore be hereby marked *advertisement* in accordance with 18 U.S.C. Section 1734 solely to indicate this fact.

Received June 11, 2018; revised September 7, 2018; accepted October 22, 2018; published first October 25, 2018.

References

1. Lee M, Lee JS. Exploiting tumor cell senescence in anticancer therapy. BMB Rep 2014;47:51–9.
2. Knizhnik AV, Roos WP, Nikolova T, Quiros S, Tomaszowski KH, Christmann M, et al. Survival and death strategies in glioma cells: autophagy, senescence and apoptosis triggered by a single type of temozolomide-induced DNA damage. PLoS One 2013;8:e55665.
3. Hirose Y, Berger MS, Pieper RO. Abrogation of the Chk1-mediated G(2) checkpoint pathway potentiates temozolomide-induced toxicity in a p53-independent manner in human glioblastoma cells. Cancer Res 2001;61:5843–9.
4. Hirose Y, Berger MS, Pieper RO. p53 effects both the duration of G2/M arrest and the fate of temozolomide-treated human glioblastoma cells. Cancer Res 2001;61:1957–63.
5. Gunther W, Pawlak E, Damasceno R, Arnold H, Terzis AJ. Temozolomide induces apoptosis and senescence in glioma cells cultured as multicellular spheroids. Br J Cancer 2003;88:463–9.
6. Stupp R, Mason WP, van den Bent MJ, Weller M, Fisher B, Taphoorn MJ, et al. Radiotherapy plus concomitant and adjuvant temozolomide for glioblastoma. N Engl J Med 2005;352:987–96.
7. Kaina B, Christmann M, Naumann S, Roos WP. MGMT: key node in the battle against genotoxicity, carcinogenicity and apoptosis induced by alkylating agents. DNA Repair 2007;6:1079–99.
8. Quiros S, Roos WP, Kaina B. Rad51 and BRCA2–New molecular targets for sensitizing glioma cells to alkylating anticancer drugs. PLoS One 2011;6:e27183.
9. Roos WP, Batista LF, Naumann SC, Wick W, Weller M, Menck CF, et al. Apoptosis in malignant glioma cells triggered by the temozolomide-induced DNA lesion O6-methylguanine. Oncogene 2007;26:186–97.
10. Tomicic MT, Meise R, Aasland D, Berte N, Kitzinger R, Kramer OH, et al. Apoptosis induced by temozolomide and nimustine in glioblastoma cells is supported by JNK/c-Jun-mediated induction of the BH3-only protein BIM. Oncotarget 2015;6:33755–68.
11. Christmann M, Diesler K, Majhen D, Steigerwald C, Berte N, Freund H, et al. Integrin alphaVbeta3 silencing sensitizes malignant glioma cells to temozolomide by suppression of homologous recombination repair. Oncotarget 2017;8:27754–71.
12. Hayflick L. The limited *in vitro* lifetime of human diploid cell strains. Exp Cell Res 1965;37:614–36.

13. Beausejour CM, Krtolica A, Galimi F, Narita M, Lowe SW, Yaswen P, et al. Reversal of human cellular senescence: roles of the p53 and p16 pathways. EMBO J 2003;22:4212–22.
14. Michishita E, Nakabayashi K, Ogino H, Suzuki T, Fujii M, Ayusawa D. DNA topoisomerase inhibitors induce reversible senescence in normal human fibroblasts. Biochem Biophys Res Commun 1998;253:667–71.
15. Chitikova ZV, Gordeev SA, Bykova TV, Zubova SG, Pospelov VA, Pospelova TV. Sustained activation of DNA damage response in irradiated apoptosis-resistant cells induces reversible senescence associated with mTOR downregulation and expression of stem cell markers. Cell Cycle 2014;13:1424–39.
16. d'Adda di Fagagna F. Living on a break: cellular senescence as a DNA-damage response. Nat Rev Cancer 2008;8:512–22.
17. Christmann M, Nagel G, Horn S, Krahn U, Wiewrodt D, Sommer C, et al. MGMT activity, promoter methylation and immunohistochemistry of pretreatment and recurrent malignant gliomas: a comparative study on astrocytoma and glioblastoma. Int J Cancer 2010;127:2106–18.
18. Wischhusen J, Naumann U, Ohgaki H, Rastinejad F, Weller M. CP-31398, a novel p53-stabilizing agent, induces p53-dependent and p53-independent glioma cell death. Oncogene 2003;22:8233–45.
19. Christmann M, Kaina B. Nuclear translocation of mismatch repair proteins MSH2 and MSH6 as a response of cells to alkylating agents. J Biol Chem 2000;275:36256–62.
20. Christmann M, Tomicic MT, Aasland D, Berdelle N, Kaina B. Three prime exonuclease I (TREX1) is Fos/AP-1 regulated by genotoxic stress and protects against ultraviolet light and benzo(a)pyrene-induced DNA damage. Nucleic Acids Res 2010;38:6418–32.
21. Christmann M, Tomicic MT, Kaina B. Phosphorylation of mismatch repair proteins MSH2 and MSH6 affecting MutS{alpha} mismatch-binding activity. Nucleic Acids Res 2002;30:1959–66.
22. Eich M, Roos WP, Nikolova T, Kaina B. Contribution of ATM and ATR to the resistance of glioblastoma and malignant melanoma cells to the methylating anticancer drug temozolomide. Mol Cancer Ther 2013;12:2529–40.
23. Peng CY, Graves PR, Thoma RS, Wu Z, Shaw AS, Piwnica-Worms H. Mitotic and G2 checkpoint control: regulation of 14-3-3 protein binding by phosphorylation of Cdc25C on serine-216. Science 1997;277:1501–5.
24. Xiao Z, Chen Z, Gunasekera AH, Sowin TJ, Rosenberg SH, Fesik S, et al. Chk1 mediates S and G2 arrests through Cdc25A degradation in response to DNA-damaging agents. J Biol Chem 2003;278:21767–73.
25. Tomicic MT, Christmann M, Kaina B. Topotecan-triggered degradation of topoisomerase I is p53-dependent and impacts cell survival. Cancer Res 2005;65:8920–6.
26. Fiorentino FP, Symonds CE, Macaluso M, Giordano A. Senescence and p130/Rbl2: a new beginning to the end. Cell Res 2009;19:1044–51.
27. Hartmann C, Kluwe L, Lucke M, Westphal M. The rate of homozygous CDKN2A/p16 deletions in glioma cell lines and in primary tumors. Int J Oncol 1999;15:975–82.
28. Iwasa H, Han J, Ishikawa F. Mitogen-activated protein kinase p38 defines the common senescence-signalling pathway. Genes Cells 2003;8:131–44.
29. Coppe JP, Desprez PY, Krtolica A, Campisi J. The senescence-associated secretory phenotype: the dark side of tumor suppression. Annu Rev Pathol 2010;5:99–118.
30. Ren B, Cam H, Takahashi Y, Volkert T, Terragni J, Young RA, et al. E2F integrates cell cycle progression with DNA repair, replication, and G(2)/M checkpoints. Genes Dev 2002;16:245–56.
31. Cam H, Balciunaite E, Blais A, Spektor A, Scarpulla RC, Young R, et al. A common set of gene regulatory networks links metabolism and growth inhibition. Mol Cell 2004;16:399–411.
32. Quiros S, Roos WP, Kaina B. Processing of O6-methylguanine into DNA double-strand breaks requires two rounds of replication whereas apoptosis is also induced in subsequent cell cycles. Cell Cycle 2010;9:168–78.
33. Gire V, Dulic V. Senescence from G2 arrest, revisited. Cell Cycle 2015; 14:297–304.
34. Baus F, Gire V, Fisher D, Piette J, Dulic V. Permanent cell cycle exit in G2 phase after DNA damage in normal human fibroblasts. EMBO J 2003; 22:3992–4002.
35. Charrier-Savournin FB, Chateau MT, Gire V, Sedivy J, Piette J, Dulic V. p21-Mediated nuclear retention of cyclin B1-Cdk1 in response to genotoxic stress. Mol Biol Cell 2004;15:3965–76.
36. Krenning L, Feringa FM, Shaltiel IA, van den Berg J, Medema RH. Transient activation of p53 in G2 phase is sufficient to induce senescence. Mol Cell 2014;55:59–72.
37. Mullers E, Silva Cascales H, Jaiswal H, Saurin AT, Lindqvist A. Nuclear translocation of Cyclin B1 marks the restriction point for terminal cell cycle exit in G2 phase. Cell Cycle 2014;13:2733–43.
38. Bunz F, Dutriaux A, Lengauer C, Waldman T, Zhou S, Brown JP, et al. Requirement for p53 and p21 to sustain G2 arrest after DNA damage. Science 1998;282:1497–501.
39. Lossaint G, Besnard E, Fisher D, Piette J, Dulic V. Chk1 is dispensable for G2 arrest in response to sustained DNA damage when the ATM/p53/p21 pathway is functional. Oncogene 2011;30:4261–74.
40. Thanasoula M, Escandell JM, Suwaki N, Tarsounas M. ATM/ATR checkpoint activation downregulates CDC25C to prevent mitotic entry with uncapped telomeres. EMBO J 2012;31:3398–410.
41. Wang D, Berglund A, Kenchappa RS, Forsyth PA, Mule JJ, Etame AB. BIRC3 is a novel driver of therapeutic resistance in glioblastoma. Sci Rep 2016; 6:21710.
42. Polager S, Kalma Y, Berkovich E, Ginsberg D. E2Fs up-regulate expression of genes involved in DNA replication, DNA repair and mitosis. Oncogene 2002;21:437–46.
43. Roos WP, Christmann M, Fraser ST, Kaina B. Mouse embryonic stem cells are hypersensitive to apoptosis triggered by the DNA damage O(6)-methylguanine due to high E2F1 regulated mismatch repair. Cell Death Differ 2007;14:1422–32.
44. Mjelle R, Hegre SA, Aas PA, Slupphaug G, Drablos F, Saetrom P, et al. Cell cycle regulation of human DNA repair and chromatin remodeling genes. DNA Repair 2015;30:53–67.
45. Silva AO, Dalsin E, Onzi GR, Filippi-Chiela EC, Lenz G. The regrowth kinetic of the surviving population is independent of acute and chronic responses to temozolomide in glioblastoma cell lines. Exp Cell Res 2016; 348:177–83.
46. Alvino E, Castiglia D, Caporali S, Pepponi R, Caporaso P, Lacal PM, et al. A single cycle of treatment with temozolomide, alone or combined with O (6)-benzylguanine, induces strong chemoresistance in melanoma cell clones *in vitro*: role of O(6)-methylguanine-DNA methyltransferase and the mismatch repair system. Int J Oncol 2006;29:785–97.
47. Felsberg J, Thon N, Eigenbrod S, Hentschel B, Sabel MC, Westphal M, et al. Promoter methylation and expression of MGMT and the DNA mismatch repair genes MLH1, MSH2, MSH6 and PMS2 in paired primary and recurrent glioblastomas. Int J Cancer 2011;129:659–70.
48. Stark AM, Doukas A, Hugo HH, Hedderich J, Hattermann K, Maximilian Mehdorn H, et al. Expression of DNA mismatch repair proteins MLH1, MSH2, and MSH6 in recurrent glioblastoma. Neurol Res 2015;37:95–105.
49. Dosch J, Christmann M, Kaina B. Mismatch G-T binding activity and MSH2 expression is quantitatively related to sensitivity of cells to methylating agents. Carcinogenesis 1998;19:567–73.
50. McFaline-Figueroa JL, Braun CJ, Stanciu M, Nagel ZD, Mazzucato P, Sangaraju D, et al. Minor changes in expression of the mismatch repair protein MSH2 exert a major impact on glioblastoma response to temozolomide. Cancer Res 2015;75:3127–38.
51. Filippi-Chiela EC, Thome MP, Bueno e Silva MM, Pelegrini AL, Ledur PF, Garicochea B, et al. Resveratrol abrogates the temozolomide-induced G2 arrest leading to mitotic catastrophe and reinforces the temozolomide-induced senescence in glioma cells. BMC Cancer 2013;13:147.
52. Kirkland JL, Tchkonia T, Zhu Y, Niedernhofer LJ, Robbins PD. The clinical potential of senolytic drugs. J Am Geriatr Soc 2017;65:2297–301.